CFD SIMULATION OF A TWIN SCREW EXPANDER INCLUDING LEAKAGE FLOWS

Rainer ANDRES[1]*, Jan HESSE[1], Haris BABIC[1], Uwe SALECKER[1], Andreas SPILLE-KOHOFF[1]
Alexander NIKOLOV[2], Andreas BRUEMMER[2]

[1]CFX Berlin Software GmbH,
Berlin, Germany
rainer.andres@cfx-berlin.de

[2]TU Dortmund University, Faculty of Mechanical Engineering, Chair of Fluidics
Dortmund, Germany
andreas.bruemmer@tu-dortmund.de

* Corresponding Author

ABSTRACT

The numerical simulation of rotary positive displacement (PD) machines has proven to be a very challenging task characterized by complex geometries with a time dependent change of the chamber volume along with complex flow physics. In addition, the leakage flow caused by housing clearances, front gaps and the intermesh clearance is of particular interest. The resulting losses have a severe impact on the overall machine efficiency.

This paper shows workflow and results for Computational Fluid Dynamics (CFD) simulations of the Screw Expander SE-51.2 of TU Dortmund University. The simulation is performed using ANSYS CFX, where the computational grids for the rotary parts are derived from the grid generator TwinMesh. The SE-51.2 is a gearless, dry running twin screw expander that converts thermal into mechanical energy by decompressing air with pressure-ratios up to 6:1 by a rotational speed range up to 20,000 rev/min. The volume ratio of the expander is 2.5 at a shaft distance of 51 mm with a displaced volume per male rotor revolution of 285 cm³. The numerical model of this machine includes fully resolved clearances along with the meshing of the rotor solid end faces whereas a contact point between the rotors is neglected. For several rotational speeds, CFD results are compared to measurements at 4 bar at the high pressure side, expanding air down to 1 bar.

The validation is based on integral values, e.g. mass flow, torque and power, all averaged over a certain time period for several operating points. Moreover, time-resolved pressure measurements for distinct positions are compared to simulation results. Besides direct evaluation against experimental data, tendencies are analyzed by varying the numerical model with respect to mesh resolution or changing the size of clearances. Apart from local changes in the flow field, it is shown that also global values like torque or mass flow are clearly affected. In addition, flow regimes not captured by measurements, like leakage flows within clearances between rotors and housing, are evaluated and illustrated based on CFD results.

While the simulation allows reliable analysis of dry running screw machines and their complex flow characteristics, oil- or water-injected machines are also commonly used in the industry, allowing higher pressure-ratios. The liquid fluid acts as a sealing for clearances and can also be used as lubricant. From the simulation point of view, multiphase calculations with corresponding multiphase-effects are required in order to cope with injected screw machines. Further investigation also involves heat transfer and resulting deformations of rotary and stationary parts. Clearances can vary due to deformations, eventually resulting in different machine characteristics and efficiency. Thus, fluid-structure interaction is of high demand. For both of these issues, a prospect is given to extend the scope of application, using CFD for screw machine analysis.

1. INTRODUCTION

Different theoretical approaches for the calculation of the operational behavior of rotary PD machines have been reported in the literature. At the Chair of Fluidics, a simulation tool KaSim was developed for the simulation of rotary displacement machines based on a zero dimensional chamber model. The calculation by the time-stepping method is made under consideration of the law of conservation of mass and energy, Janicki (2007). For the purpose of simplicity, it is assumed that spatial gradients in the intensive state variables are negligibly small and the fluid condition within a working chamber can thus be regarded as homogeneous. Hereby, a 3D CFD method is essential, if the spatial distribution of the variables of state is required. By means of an iterative fluid-structural interaction coupling of KaSim und the Finite Element Method (FEM) program ANSYS, the calculation of temperature distribution in the components as well as resulting thermal deformation, was presented by Nikolov et al. (2012). The automation capability is given due to the ANSYS Parametric Design Language (in short: APDL). A dynamic model for the performance prediction of a twin screw expander was presented by Papes et al. (2015). Here, the calculation approach was compared to 3D CFD simulations.

The geometry of the test screw expander SE 51.2 used to validate the simulation model within the framework of this paper is presented by Nikolov and Brümmer (2016). SE 51.2 is a dry-running screw-type expander prototype without timing gear designed at the Chair of Fluidics by Temming (2007). In order to avoid damage in the rotor intermesh due to the lack of lubrication, both rotors are hardened and have a tough wear-protection coating are. Characteristic for SE 51.2 are its relatively small dimensions and high rotational speed up to 20,000 rev/min at operation.

2. CHAMBER MODELING

The modelling of rotation and deformation of the fluid domain between rotors and housing is the most challenging task in order to get a numerical representation of the PD machine. Here, the mesh generator TwinMesh is used to create the numerical grids for the fluid domain. The time dependent change of the chamber volume according to the rotor position is modelled by creating meshes for each rotor position. For the SE-51.2 twin screw expander, the chamber volumes of two axially parallel rotors are meshed with O-type grids for each rotor, using hexahedral elements, as shown in Figure 1. These O-type grids cover the fluid volume which is determined from the 2D rotor and housing contours.

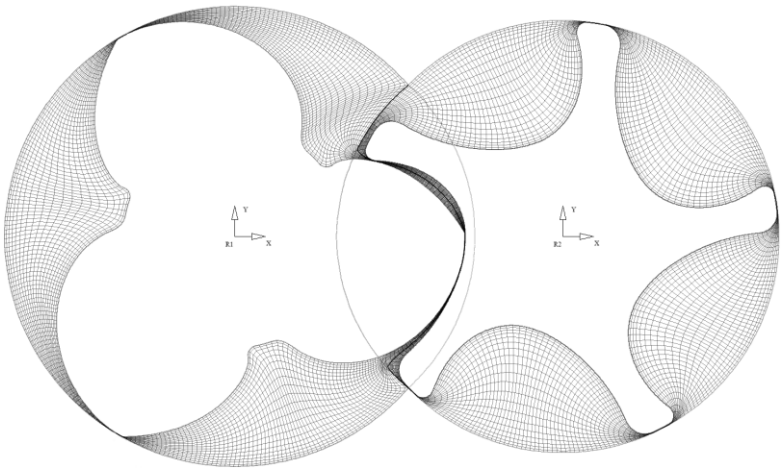

Figure 1: Grid on a 2D cross section of the male (left) and female (right) rotor

The twisted rotor geometry along the axial direction (200° twist angle for male rotor, 120° for female rotor) is modelled by a consecutive staggering of 2D mesh sections. For each axial position, 3D grids are created, which satisfy specific quality criteria. The minimum element angle is above 18°, the aspect ratio below 2000 and volume change below 20. Towards housing and rotor walls, the grid is refined to have an adequate boundary layer resolution. The 3D meshes are exported from TwinMesh for each rotor position (i.e. the meshes cover a periodic section of 120° in this case), where an angle increment of 1° is used for the simulation of the SE-51.2 screw expander. A more detailed description of the mesh generation using TwinMesh is given by Hesse (2016). The

stationary fluid domains, i.e. suction and discharge port as well as inlet and outlet pipes are provided as separate meshes. These are generated using ANSYS Meshing and ANSYS ICEM CFD. In this case, hexahedral elements are used for the inlet and outlet pipes, whereas tetrahedral elements are used to mesh the more complex geometry of fluid regions around the suction and discharge port.

3. SIMULATION SETUP

The simulation is carried out in ANSYS CFX, where the simulation setup contains the assembly of all stationary and rotary fluid regions, see Figure 2 (right). The grids for the rotary parts also include the fluid regions for all clearances. All meshes are connected via fluid-fluid interfaces, where the flux of mass, momentum, heat and turbulence is conserved. In addition, appropriate boundary conditions are defined, representing the desired operation point. For the screw expander, pressure and temperature at inlet and outlet are set as well as the rotation speed of the male rotor. Apart from interfaces, inlet and outlet faces, no slip walls are assigned.

For the simulation of rotary PD machines, especially the mesh motion due to the rotor rotation and thus the deformation of the chamber volume is of interest. This is realized by using a FORTRAN routine, which loads the new mesh information (according to the current rotor position) at the beginning of each simulated time step. In the ANSYS CFX solver, the mesh deformation is added to the set of differential equations, so that no interpolation is required between time steps. The constrained pressure at inlet and outlet of the numerical model can lead to an artificial pressure reflection, most distinct at the high pressure side (i.e. inlet side of the expander). These waves affect the pressure and velocity field and represent an undesired discrepancy between numerical and real model. In all simulations performed, the distortion of monitored flow quantities caused by those pressure waves is prevented by using non-reflective boundary conditions, allowing the pressure waves to pass the artificial inlet and outlet boundaries.

In this paper, for a pressure ratio of 4:1 with an air inflow temperature of 90°C, the expander is simulated for several rotational speeds between 1,000 and 16,000 rev/min. For the reference operating point at 4,000 rev/min, a variation of the numerical model is performed. As a geometric variation, one simulation with 25% increase of radial clearances (housing gap, intermesh clearance and blow hole) and one simulation with 25% increase of axial clearances (front gaps) are carried out. Also a simulation with a decreased mesh resolution is performed, decreasing the total amount of elements from about 920,000 down to approximately 52,000 per rotor chamber. Because the sharp and most distinct pressure and velocity gradients are expected to occur within the moving rotor chambers (especially in narrow clearances), the grids for those chambers are assumed to outweigh the stator meshes with regard to their impact on flow characteristics. Thus, rotor meshes are coarsened in the radial, axial and circumferential direction, whereas coarsening of the stator grids is only applied at the interface regions. In this way, discontinuities regarding the element sizes in regions where rotary and stationary parts connect to each other are prevented.

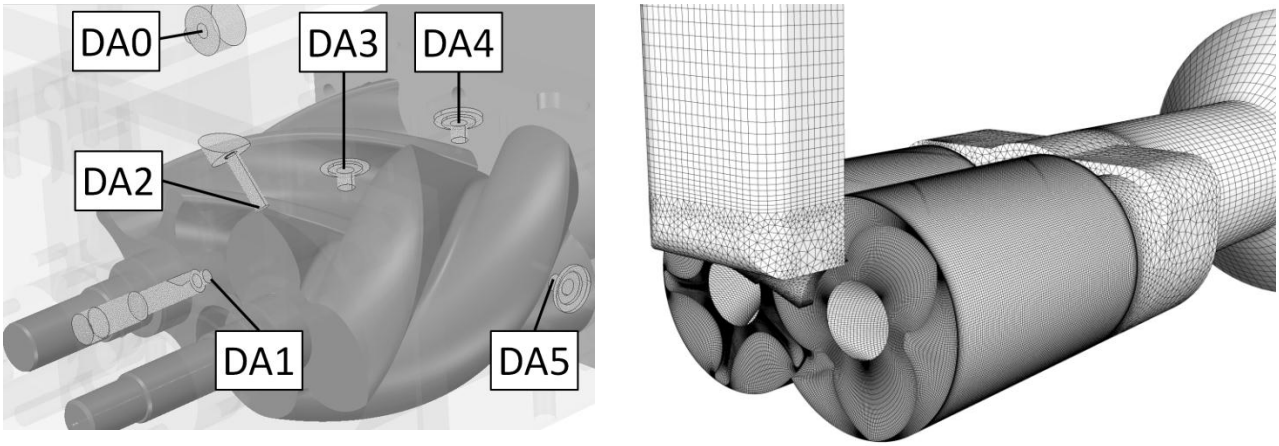

Figure 2: CAD model of the SE-51.2 screw expander including pressure measurement points (left) and assembly of rotary and stationary mesh regions including meshes for the front gap clearances (right)

4. SIMULATION RESULTS

The flow conditions inside the screw expander are visualized by a contour plot of the instantaneous pressure and velocity fields. These spatially resolved results are shown for a specific rotation angle, i.e. for a specific point in time. Time resolved results refer to a periodic solution over time, i.e. for a converged simulation, the monitored flow quantities are periodic over a section of 120° (due to rotational periodicity of the rotors). The gas enters the expander at a pressure of 4 bar, filling the pressure chamber between the flanks of male and female rotor. The screwed rotors form several chambers in axial direction, where the volume of the chamber is increasing with the rotation angle. Because of the pressure inside those chambers acting on the rotor walls, the fluid energy is converted into mechanical energy, represented by the torque of the rotors. This is illustrated in Figure 3 for three different male rotation angles over a periodic section of 120°.

At a rotation angle of 40°, both rotors reach the control edge of the pressure port. At this point in time, the filling process of the preceding chamber (2) has finished, since there is no longer a connection between pressure port and chamber (if clearances are neglected). With further rotation of the rotors, the foremost chamber (1) fills up with air, causing a pressure on the rotor walls of 4 bar, while the chamber volume is increasing simultaneously. At the same time, in chamber (2) a pressure of about 3 to 3.4 bar is calculated.

For a rotation angle of 80° and 120° respectively, the pressure on the rotors in chamber (1) remains nearly constant at 4 bar, because there is an ongoing supply with inflowing air through the pressure port. In chamber (2) on the other hand, pressure is dropping over rotation angle because of the increasing chamber volume. Once the lobes of both rotors reach the control edges again, the air supply of chamber (1) is cut and pressure also starts to decrease, while a new chamber is already formed. Due to the rotational symmetry, the 40° position in Figure 3 can be interpreted as the subsequent position 160°, where the aforementioned pressure drop of chamber (1) can be observed.

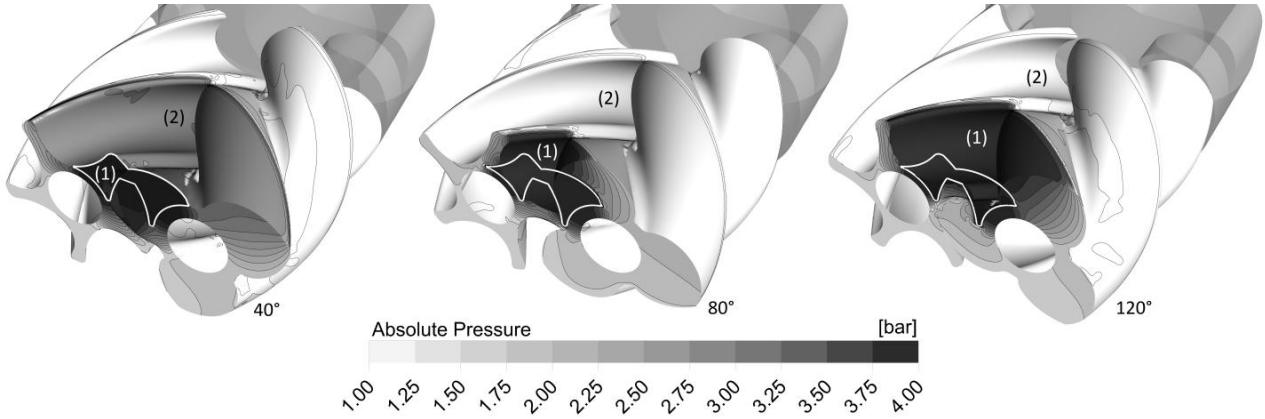

Figure 3: Pressure distribution at 4,000 rev/min on the rotors for male rotation angle of 40°, 80° and 120°

This work mechanism of the screw expander can be also demonstrated in Figure 4. Regarding the averaged chamber pressure over rotation angle for the reference operation point (4,000 rev/min, pressure-ratio of 4:1, air inflow temperature of 90°C), a pressure drop can be noticed at less than 160°, i.e. before the lobes reach the control edge. The cross section area of the pressure port through which chamber (1) is supplied with air is decreasing past 120° of rotation. In dependence of the rotation speed, sufficient replenishment with air to maintain a pressure of 4 bar is not given. This represents a throttle effect with a growing influence on the chamber fill level at increasing rotation speeds. Hence, at a lower rotation speed of 1,000 rev/min, this throttle effect is less pronounced, as the pressure drop is deferred to a higher rotation angle or a higher chamber volume, respectively.

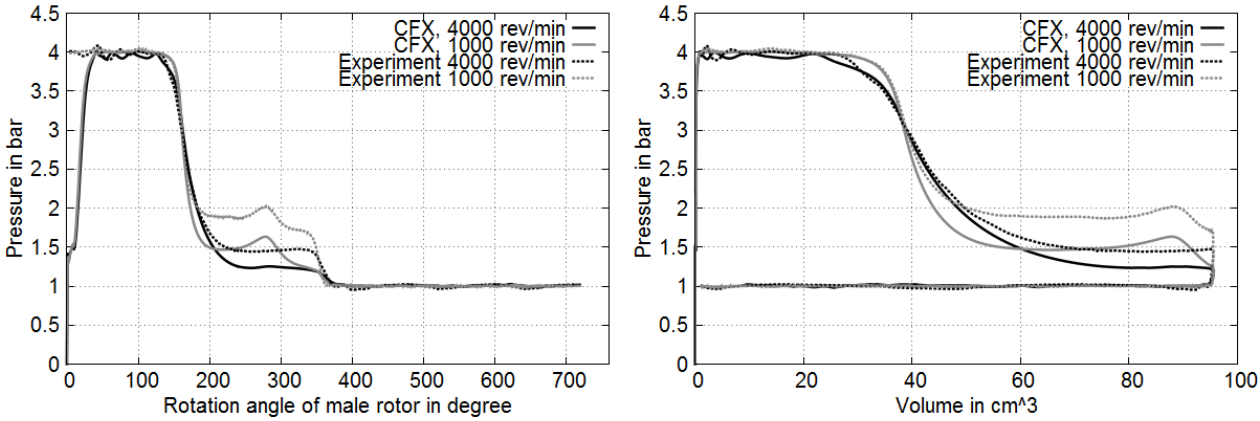

Figure 4: Averaged chamber pressure over male rotation angle (left) and over chamber volume (right) for experimental measurements and simulation results at 1,000 rev/min and 4,000 rev/min

Comparing simulation with experiment, results are qualitatively in good agreement. Nevertheless, chamber pressure measurements only cover male rotation angles higher than 45°. For lower angles, the pressure is estimated, e.g. according to the inlet valve pressure, whereas simulation results cover the entire angle range. Past 45°, filling process and pressure drop pressure due to the expansion of the chamber are in good match as well as the chamber refill seen at 1,000 rev/min for a chamber volume higher than 40 cm³. This effect occurs for lower rotation speeds, where caused by leakage, the chamber is refilled with air from regions with higher pressure, resulting in a pressure rise before discharge. The noticeable difference between simulation and experiment can be seen in the lower pressure level, which is reached through chamber expansion. For a fully expanded chamber at 1,000 rev/min, the difference is approximately 0.4 bar, whereas for 4,000 rev/min the difference is 0.25 bar. It is conceivable that the smaller pressure drop measured in the experiment is caused by the leakage through the rotor bearings, which affects rotation angles from 200° till discharge. This leakage is quantified in the experiment by 7.2 kg/h and represents an additional rotor chamber inflow, which was not modeled in the simulation.

Figure 5 compares the measured and calculated pressure distribution over an angle range of 240° at distinct pressure measuring points. The positions of the individual points can be derived from Figure 2 (left). The calculated results are found to be in very good agreement with the experiment. However, point DA4 shows the abovementioned difference in the pressure level through chamber expansion. The mean deviation at this pressure point is about 0.2 to 0.25 bar, which fits well to the results presented earlier in Figure 4.

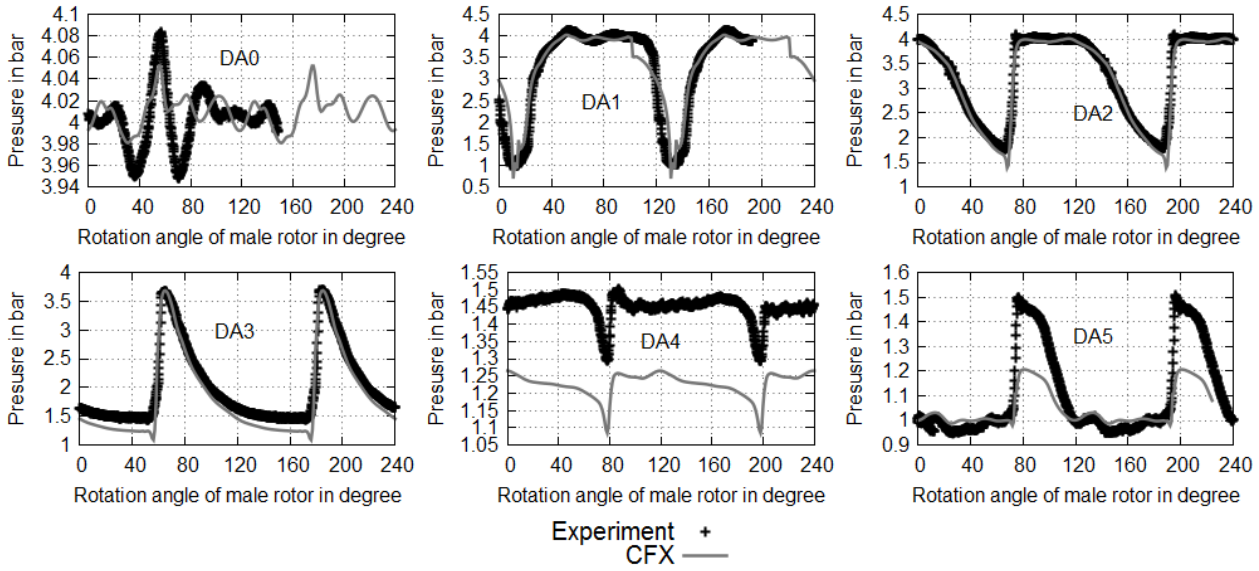

Figure 5: Measured and calculated pressure at measuring points DA0 to DA6 at 4,000 rev/min

The velocity field in Figure 6 shows the flow pattern within rotor chambers and housing. As illustrated, the velocity upstream and downstream of the rotor chamber varies between 10 m/s and 25 m/s. Within the rotor chamber, higher velocities are present while the maxima are located within clearances. Examplified in Figure 7, velocities above 200 m/s up to 500 m/s are illustrated at a wall distance of 0.02 mm from the rotor walls. These high velocities occur primarily within the front and housing gaps at the high pressure side. Also the blow hole causes leackage flow. This can be visualized in Figure 8, where the leackage flow through the blow hole is evident. Caused by the pressure difference between chambers in the the axial direction, a jet of high pressurized air streams into the chamber with a lower pressure level. At the investigated reference operation point, the peak velocity of jet through the foremost blow hole is approximately Ma =1.2.

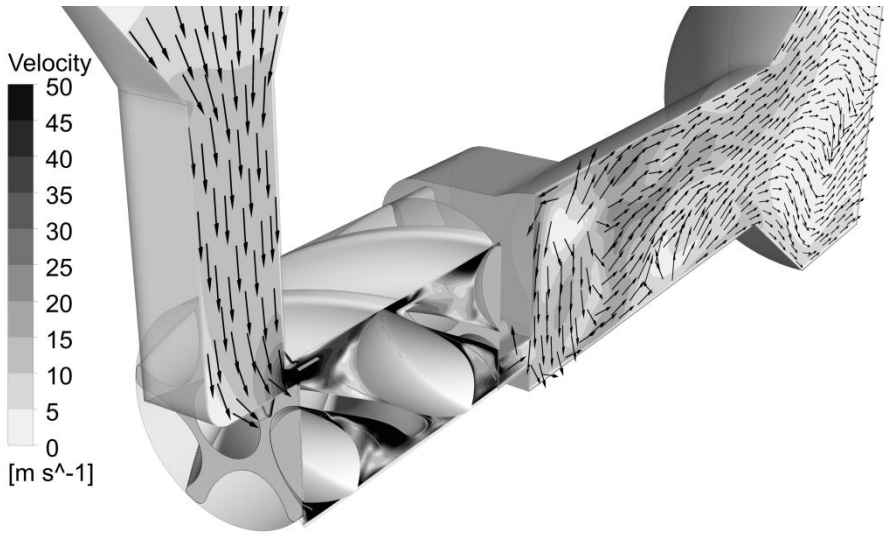

Figure 6: Contour plot of the velocity field at male rotation angle of 0° at 4,000 rev/min

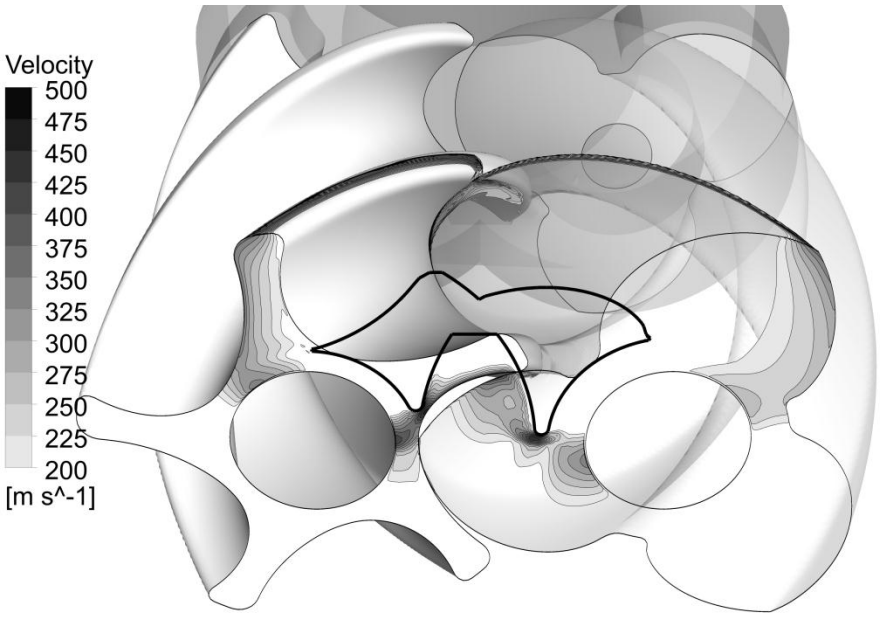

Figure 7: Flow regions with a velocity above 200 m/s at male rotation angle of 0° at 4,000 rev/min

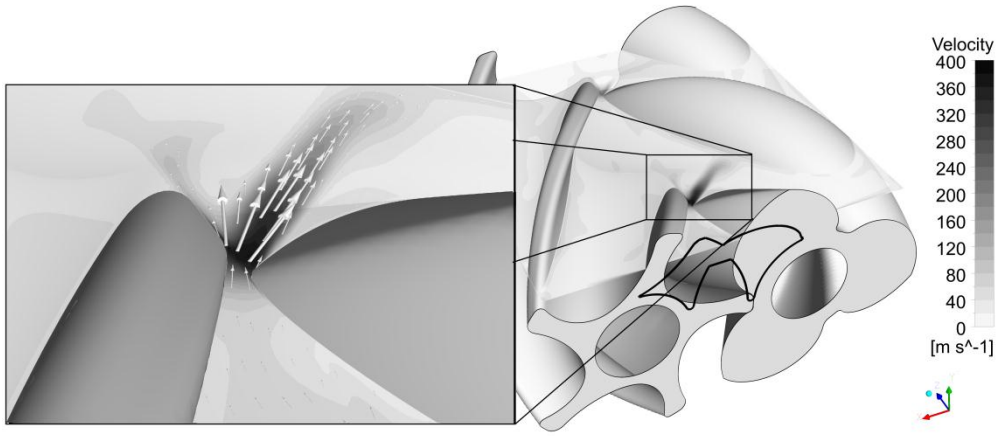

Figure 8: Velocity field on a horizontal plane, illustrating the leakage flow through the blow hole at male rotation angle of 75° at 4000 rev/min

Since leakage flow does partially not contribute to the conversion of thermal energy into mechanical energy, it has an adverse impact on the efficiency and overall performance of the screw expander. In the simulation, it can be demonstrated on the basis of integral values like mass flow (at inlet and outlet) and generated power. Figure 9 depicts the calculated results for these quantities on the basis of varied radial clearances. The case with 80 µm housing gap represents the reference case according to measured gaps on the real machine. As a variation of the model, housing clearance is increased by 25% (i.e. from 80 to 100 µm) for both rotors. Due to a normal rotor scaling of 20 µm to increase the housing gap, also the average intermesh clearance is increased, resulting in a larger blow hole as well. Comparing the results for both gap sizes, the higher mass flow caused by higher leakage is apparent. Averaging the mass flow over one revolution, the case with larger radial clearances exceeds the reference case by approximately 12%. Comparing the same cases in terms of generated power, the difference is smaller but still noticeable. The deviation is about 2 % for total power.

Figure 10 compares averaged results for mass flow and generated power for a rotational speed range between 1,000 and 16,000 rev/min with measurements. Also, the cases with the model variations (i.e. increased clearances, decreased rotor grid resolution) are included. For the reference point at 4,000 rev/min, a mass flow of 180 kg/h was measured, whereas 167 kg/h are calculated by the simulation (without model variation). Concerning the generated power, only the inner power is compared, i.e. bearing friction and friction caused by contact of rotor lobes are neglected. The measured value is 2,973 W, while the calculation yields 2,808 W. Regarding the model variation, the increase of front gaps shows a minor impact on the mass flow, which raised by nearly 3% (compared to 12% caused by increasing radial gaps). This is also the case for the generated power, where the larger front gaps results in only 0.5% (compared to 6.5% for increased radial gaps) change compared to the reference front gap size. The calculation on coarsened rotor grids however shows a significant deviation from both, measurement and reference CFD results. Despite unchanged clearances, the coarsened grids lead to a mass flow of 215 kg/h, which is off by over 28% regarding the fine grid results. As for generated power, the difference is about 12.5% using the coarse rotor grids.

It can be seen that both, mass flow and power are slightly underestimated by the simulation over the investigated range of operation points. However, with regard to the variation of the rotation speed, the trend of resulting mass flow and power shows a very good match with the measurements. The mean deviation between CFD results and measurements can be quantified as approximately -8 % for mass flow and -7% for generated power. Figure 11 presents a quantification of the leakage flow through radial clearances (including housing clearance, intermesh clearance and blow hole) and front gaps for the male rotor over a rotation period of 120° for both, reference and increased radial clearances. For the reference gaps, the average leakage through the front gap (only high pressure side) is approximately 1.2 kg/h, whereas for radial clearances, it is about 10.8 kg/h. As aforementioned, the leakage through the rotor bearing was not included in the simulation, but quantified with 7.2 kg/h, it is near the magnitude of the housing clearance leakage. Thus, it is considered to have noticeable impact on the integral mass flow of the expander, which can contribute to the mass flow underestimation by the simulation compared to the experiment.

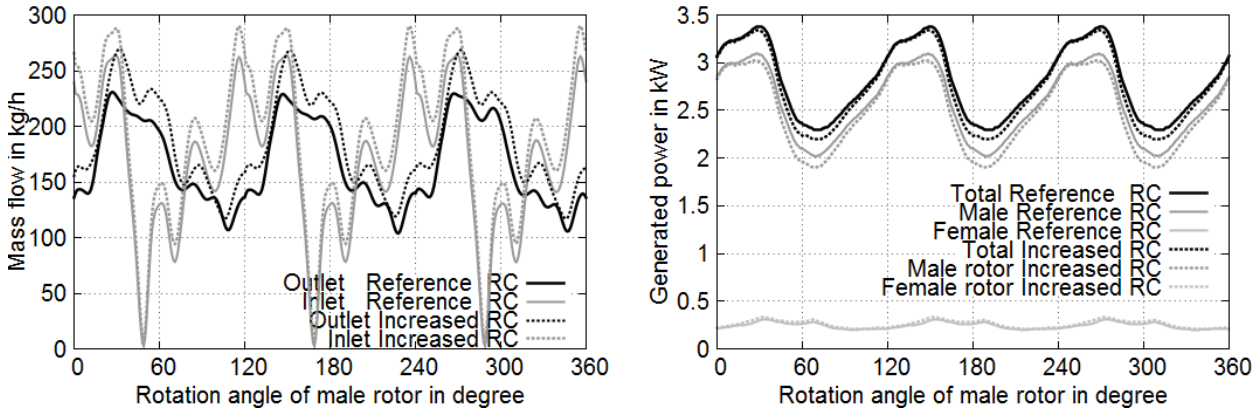

Figure 9: Comparison of Mass flow (left) and generated power (right) at 4,000 rev/min for reference and increased radial clearances (RC) over 360° of male rotor revolution

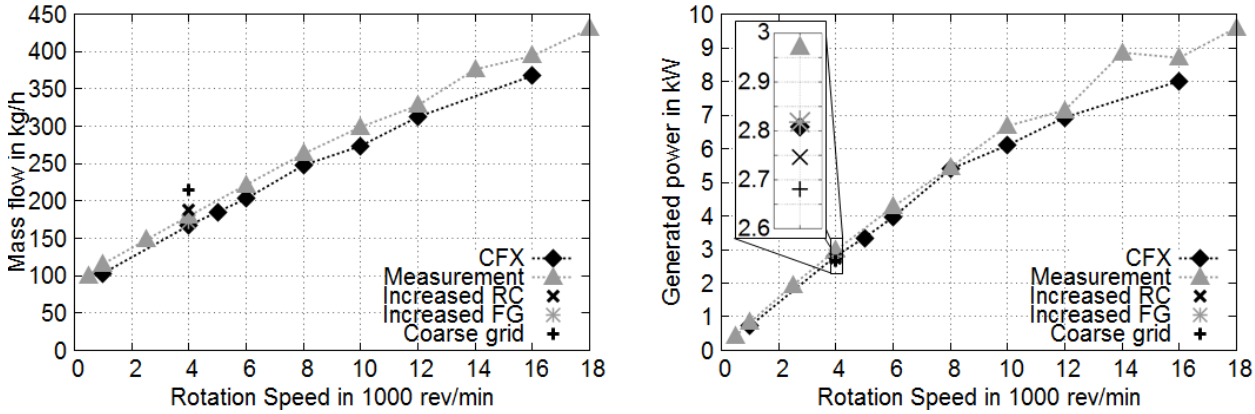

Figure 10: Comparison between CFD and measurements:
Mass flow (left) and generated power (right) for different operation points and for cases with increased radial clearances (RC) and increased front gaps (FG)

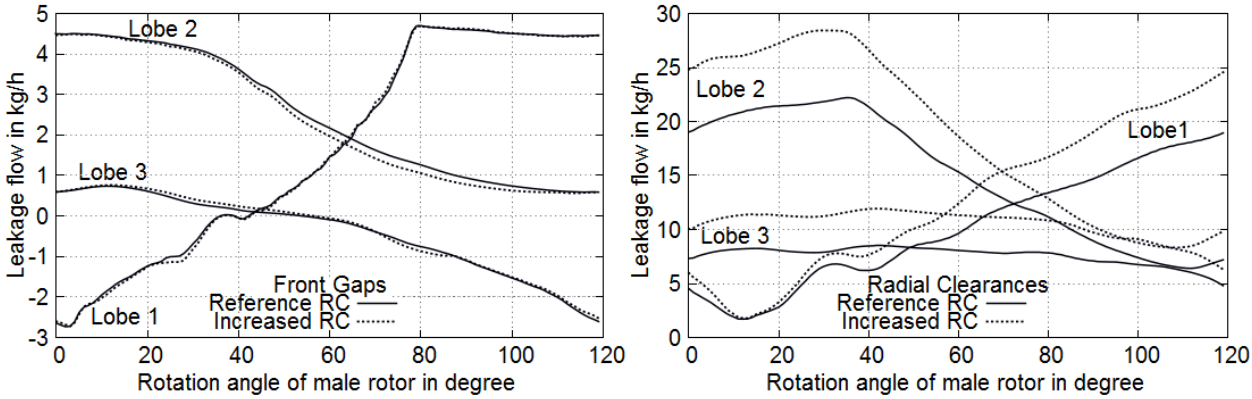

Figure 11: Front gap (left, only front gap at pressure side) and radial clearance (right) leakage flow at 4,000 rev/min for the three male rotor lobes over 120°. Comparison between reference and increased radial clearances (RC)

5. FLUID STRUCTURE INTERACTION AND MULTIPHASE SIMULATIONS

Based on the CFD results, also a one-way coupled thermal and structural analysis is performed, using ANSYS Mechanical. The numerical model for stator and rotor solids includes the definition of clamping and contact points between components, screw pretension forces, bearing positions as well as material properties. For one point in time (here the last simulated time step), the CFD results at the encasing faces of the fluid volume mesh are mapped to the corresponding faces of the stator solid mesh in ANSYS Mechanical. With the applied loads to the rotor and stator solids, the deformations and stresses in the model are calculated from a steady-state structural analysis. The results only correspond to one point in time and provide a first estimation of the deformation, which is illustrated in Figure 12. With the clamping definition applied (i.e. the clamping of the real model), the intended degree of freedom of the expander is directed along the axial direction (i.e. in z-direction). Hence, the global maximum of the calculated deformation occurs along the axial direction and is approximately 0.174 mm. Nevertheless also radial deformations (i.e. in x- and y-direction) are present. The maximum radial deformation of the rotor is about 56.96 µm, whereas the adjacent shell surface of the stator extends for approximately 56.21 µm in negative y-direction. Thus, at this location and for this point in time, the housing clearance is assumed to barely change. The maximum change in the housing gap is calculated approximately at half axial rotor length. Here the deformation of stator and clearance lead to a 13 µm reduction of the housing gap.

The outlined one-way coupling of fluid and structure could be also performed for every time step, so that time resolved deformations and stresses on the structure can be analyzed. This was not part of the current investigation and it is expected to be very time consuming, as the mapping of the CFD results for the steady-state analysis took about four hours for one time step. It should be also noted, that the applied loads do not represent the final state, as the heating of the machine takes place on a higher time frame than covered by the simulation. From experimental results, a temperature increase after more than 30 minutes is still noticeable, whereas the presented CFD results correspond to a simulated time of less than one second (i.e. the start-up of the expander and hence the first few revolutions).

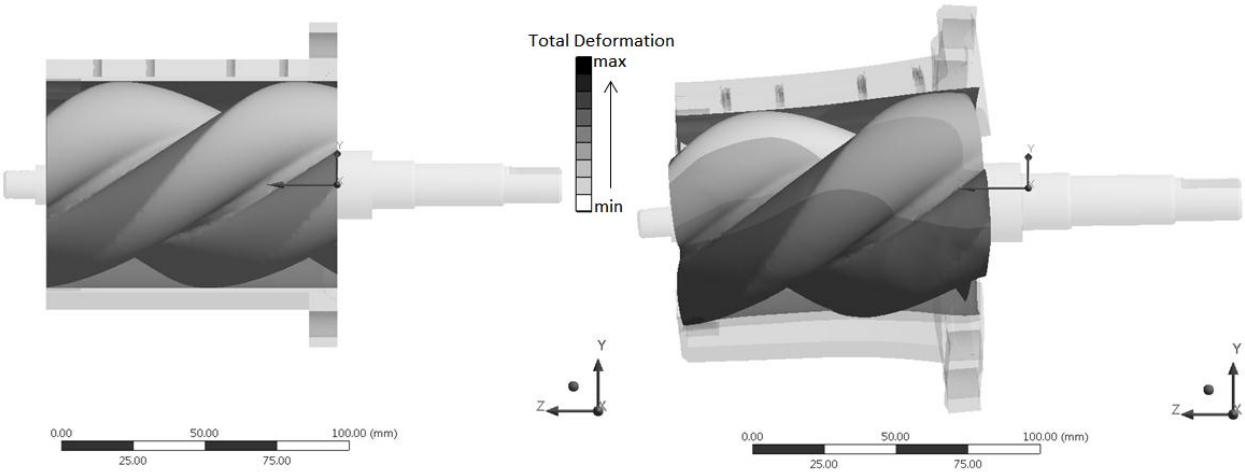

Figure 12: Qualitative deformation at 4,000 rev/min, pressure ratio 4:1 and air inflow temperature of 90°C

Another challenge is the modeling of multiphase flows, e.g. to analyze oil- or water-injected screw machines. Figure 13 shows a qualitative result of a simulation approach of an oil injected screw compressor, where oil is injected through supply valves in both rotor chambers at the pressure side. To model the multiphase flow, the volume of fluid method is used in ANSYS CFX with homogeneous coupling of gaseous and liquid phase. The presented results depict regions with an oil volume fraction higher than 1% after 6 revolutions of the male rotor. The approach demonstrates general feasibility with available multiphase models. Nevertheless, validation of oil distribution within rotor chambers as well as resulting effects like sealing or cooling is desired for well-defined operation points.

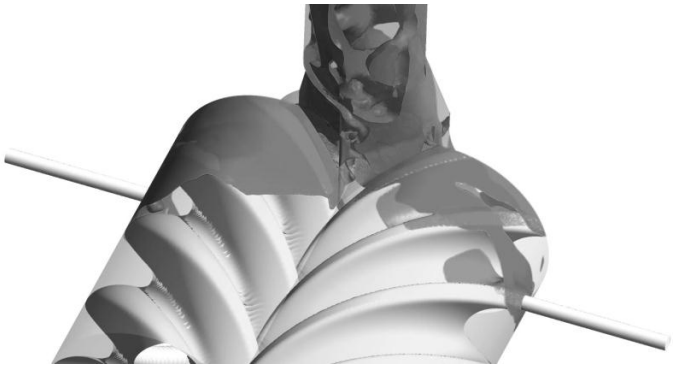

Figure 13: Simulation of an oil injected screw compressor

6. CONCLUSIONS AND OUTLOOK

The presented CFD results of the SE-51.2 twin screw expander in comparison with experimental data indicate that the working mechanism and flow conditions within the expander are well captured by the simulation. It accounts for effects like throttling, chamber refilling or leakage flows and examined flow quantities are overall in good agreement with the measurements. Moreover, the CFD easily allows analyzing tendencies, like e.g. the variation of clearances or changing the operation point. With regard to further investigations, accurate modeling of leakage sources (i.e. all clearances present in the real model) should be treated with particular attention, as it severely affects the machine characteristics. Neglecting the rotor bearing leakage in the presented numerical model is assumed to considerably contribute for fewer losses compared to the experiment, as seen in the pressure volume. Also the separate quantification of the individual leakages through radial clearances (i.e. housing gap, intermesh clearance and blow hole) is of interest. The significance of leakage modeling demands for high quality meshes at high resolutions, as coarse meshes tend to result in a decreasing accuracy regarding geometry approximation, especially the intermesh clearances of rotary PD machines. The significant overestimation of the mass flow derived from the coarsened rotor meshes can be mainly caused by an insufficient spatial resolution of clearances.

Both, fluid structure interactions as well as multiphase flows are a challenge of upcoming numerical investigations, as the numerical effort is clearly increased, especially with the aim of a two-way coupling between fluid and structure. Also procedures with the goal to shorten simulation time are to be elaborated, e.g. applicable initialization of oil initialization or the way of coupling the fluid with the structure. For all issues, there is the claim for reliable experimental results in order to validate the numerical models.

REFERENCES

Hesse, J., Spille-Kohoff, A. (2016). CFD simulation of a screw compressor including leakage flows and rotor heating. *Proceedings of the 3rd International Rotating Equipment Conference (IREC)*, Düsseldorf.

Janicki, M. (2007). Modellierung und Simulation von Rotationsverdrängermaschinen. *Dissertation*, TU Dortmund University, Dortmund.

Nikolov, A., Brümmer A. (2016). Analysis of Indicator Diagrams of a Water Injected Twin-shaft Screw-type Expander. *Proceedings of the 23st International compressor engineering conference at Purdue*, Purdue.

Nikolov, A., Huck, C. & Brümmer A. (2012). Influence of Thermal Deformation on the Characteristic Diagram of a Screw Expander in Automotive Application of Exhaust Heat Recovery. *Proceedings of the 21st International compressor engineering conference at Purdue*, Purdue.

Papes, I., Degroote, J. & Vierendeels, J. (2015). Dynamic model for the performance prediction of a twin screw expander in ORC. *Proceedings of the 3rd International Seminar on ORC Power Systems* (513-521). Brussels.

Temming, J. (2007). Stationärer und instationärer Betrieb eines unsynchronisierten Schraubenladers. *Dissertation*, TU Dortmund University, Dortmund.